Electronic structure of boron-interstitial clusters in silicon

2005 J. Phys.: Condens. Matter 17 S2141

(http://iopscience.iop.org/0953-8984/17/22/001)

INSTITUTE OF PHYSICS PUBLISHING JOURNAL OF PHYSICS: CONDENSED MATTER

J. Phys.: Condens. Matter **17** (2005) S2141–S2153 doi:10.1088/0953-8984/17/22/001

Electronic structure of boron-interstitial clusters in silicon

Peter Deák[1,2], Adam Gali[1], András Sólyom[1], Adam Buruzs[1] and Thomas Frauenheim[2]

[1] Department of Atomic Physics, Budapest University of Technology and Economics, Budafoki út 8, Budapest, H-1111, Hungary
[2] University of Paderborn, Theoretical Physics, Paderborn, D-33095, Germany

E-mail: p.deak@eik.bme.hu

Received 6 October 2004
Published 20 May 2005
Online at stacks.iop.org/JPhysCM/17/S2141

Abstract

Hybrid functional calculations within density functional theory are carried out to investigate the electronic structure of boron-interstitial clusters (BICs). A one-parameter hybrid functional is chosen is to give accurate results for the whole electronic structure (including the gap) *and* the elastic properties of crystalline silicon. It is shown that this approach provides dependable defect level positions in the gap. Investigation of the boron + vacancy and boron + self-interstitial centres gives a consistent description of the experimentally observed G10 and G28 centres. The electronic structure of BICs, which may affect the activation rate of boron implantation, are reported. The one-electron level positions of isolated B_nI_m defects are given.

(Some figures in this article are in colour only in the electronic version)

1. Introduction

Boron-interstitial clusters (BICs) are a key problem in the control of diffusion and activation of ultra-shallow boron implants in ULSI silicon device technology. Many of the boron atoms get trapped in BICs, which provide significantly fewer holes than the number of boron atoms in them. In recent years attempts have been made to determine formation and dissolution energies of the possible clusters from *first principles* theoretical calculations [1–3]; however, apparently, energy calculations alone were not sufficient to establish the key players in the clustering process of boron. As an alternative, the most important BICs could be identified based on their spectroscopic properties. The electronic structure provides a fingerprint for defects: the position of one-electron energy levels in the band gap can be measured optically or electronically, while the spatial extent of the corresponding states are accessible by magnetic resonance measurements if the defect is in a state of non-zero spin. Following on from

the calculations of the vibration spectra of a great number of BICs earlier [4], the present paper describes their electronic structure, obtained by a hybrid functional within density functional theory, to avoid the well-known 'gap' error of standard methods. There are two experimentally well documented boron defects in silicon: the boron + vacancy (Si-G10) [5] and the boron + interstitial (Si-G28) complex [6]. These are used here as test cases. In addition, the electronic structure of those BICs are presented, which were found to be important in the clustering process [2].

The usual nomenclature of BICs, B_nI_m, is based on the number n of boron atoms and the number m of interstitials involved in the cluster, irrespective of the fact that the interstitial is a boron or a silicon atom. In this notation, BI may as well mean an interstitial boron or a silicon self-interstitial next to a substitutional boron. Such systems are configurational isomers with the same number of atoms. In order to be able to differentiate among the possible isomers, the present study also uses the notations Si_i, B_i, and B_s for interstitial silicon and boron, and for substitutional boron, respectively.

2. Methods

Nowadays, density functional theory (DFT) is the most often used method for electronic structure calculations but, as is well known, all its conventional implementations, i.e., both LDA (local density approximation) and GGA (generalized gradient approximation), lead to band gaps which are lower by ∼50% than the experimental values [7, 8]. The reason is the inappropriate description of electron self-interaction in the respective exchange–correlation potentials. The application of quasi-particle corrections within the original GW method [7] is not yet possible for large systems, and even approximate GW calculations [9] are much too expensive. It has been shown that by using an exact exchange potential with any of the correlation potentials in DFT, the gap error can largely be corrected [8] but, at present, no computer code exists which would practically allow defect calculations on large supercells using such an approach either.

According to experience, the 'band gap error' of LDA and GGA manifests itself mainly in a more or less rigid shift of the conduction band (CB) states with respect to the valence band (VB) states. The error in the position of VB states is minor and the relative error among CB states is also often smaller than the error in the gap[3]. This observation has led to the introduction of the so-called 'scissor operator': a rigid shift of the CB states with respect to the VB edge [10]. Electronic states of substitutional defects can always be expanded on the complete basis of the perfect crystalline states. The scissor operator would then shift the defect levels in proportion to the contribution of CB states in the expansion. Since, in fact, the 'band gap error' concerns both bands and also relative energies in the bands, the scissor operator gives only a very rough correction, and it does not even work well for interstitial defects. Unfortunately, the error in the band gap has severe consequences on the calculated electronic (and sometimes even the geometric) structure of the defect. With the lack of an accurate correction for the CB (and of any for the VB), the level positions in the gap, calculated in the framework of LDA or GGA for complex defects, are rather uncertain. This also has an effect on comparing their formation energies. In addition, if—in extreme cases—the defect level slips into or out of the bands due to the band gap error, the calculated equilibrium geometry may be completely wrong. Shallow level defects also represent a problem [11]. Therefore, for

[3] N.B.: Typically the VB and the CB are narrower in plane wave LDA calculations than observed. The difference at the VB is small, indeed: e.g., 12.2 eV in Si, instead of 12.5 eV. However, the calculations in silicon result in 0.5 eV for the indirect band gap and 2.5 eV for the direct gap at the centre of the Brillouin zone, compared to the observed 1.2, and 4.2 eV, respectively. So the rigid shift of CB states does not always work very well.

Table 1. Position of the highest occupied orbital of the $B_{Si} + (C_i)_2$ complex in 3C-SiC with respect to the perfect crystal VB edge (in eV) in the positive and negative charge state at the centre of the Brillouin zone in a 64-atom supercell. In both cases the orbital is localized to the defect.

Charge state	LDA	GW	Hybrid functional
(+)	−0.12	+0.04	+0.10
(−)	+0.18	+0.26	+0.29

calculating defect level positions comparable to experiment, it is paramount to select a method which reproduces the electronic structure of the perfect crystal on both sides of the gap.

Due to the difficulties with the existing implementations of DFT, the calculation of excited or transition states is usually also not sufficiently accurate, while the usage of exact exchange consistently in a DFT framework is yet not practical. Because of this, the use of empirically determined hybrid potentials was suggested in quantum chemistry. The most widely applied form, the so-called B3LYP potential [12], is based on 20% mixing of the exact Hartree–Fock (HF) and a GGA exchange potential, extended with a GGA correlation potential [13]. (Also, the local and non-local parts of both potentials are empirically weighted.) Despite its semi-empirical nature, the experience in quantum chemistry is very favourable with the B3LYP potential. It has also been shown [14] that the optical band gap of solids can be calculated to a good approximation. In the specific case of silicon, our test has shown that B3LYP yields a much too large indirect band gap (1.84 eV, as compared to the value of 1.17 eV measured at low temperature). This could not be much improved upon, even if the basis set was increased. However, Becke himself suggested in a later paper [12] that useful hybrid functionals with a simple one-parameter mixing of HF and DFT exchange can be used to predict the energetics of a large set of molecules, and it was also shown [15] that, by varying the mixing parameter between the HF and the GGA (or LDA) exchange, the correct gap *and* several other properties of a solid can be 'tuned' in. This possibility has been implemented into the CRYSTAL code [16], which is capable of both HF and DFT calculations on periodic systems.

Our experience has shown that a 20% mixture of the HF exchange with the most common LDA exchange can reproduce accurately the very different band gaps of *all* polytypes of SiC [17], while giving good values for the other basic properties. A case study on a complex defect in 3C-SiC proves that the level positions obtained by this mixture are comparable with those obtained from an approximate GW [9] calculation. The complex $B_{Si} + (C_i)_2$ has two defect levels in the gap, the lower one (near the VB edge) is doubly occupied, and the higher one singly occupied in the neutral charge state. Table 1 compares the level positions with respect to the VB edge of the perfect lattice, as obtained in a pure LDA, an LDA + GW, and an LDA + 20 exact exchange calculation for the singlet (singly positive and singly negative) charge states. As can be seen, the hybrid functional mimics the effect of the GW correction well, while the pure LDA result is not even qualitatively correct for the positive charge state.

Applying the 20% mixing of HF and LDA exchange gives 1.4 eV for the indirect gap of silicon (somewhat higher than the observed 1.2 eV) and 5.0 eV for diamond (lower than the experimental 5.6 eV), so our results for SiC are somewhat fortuitous. The B3LYP functional has been determined by fitting to a large set of molecular data, and obviously a large set of solids should be considered (including the band gap into the data set) to optimize the mixing parameter of a new hybrid functional. In the present study, however, we are only concerned with defects in silicon. Enhancing the accuracy of the electronic structure calculation in silicon at the expense of transferability is, therefore, acceptable, provided the other properties

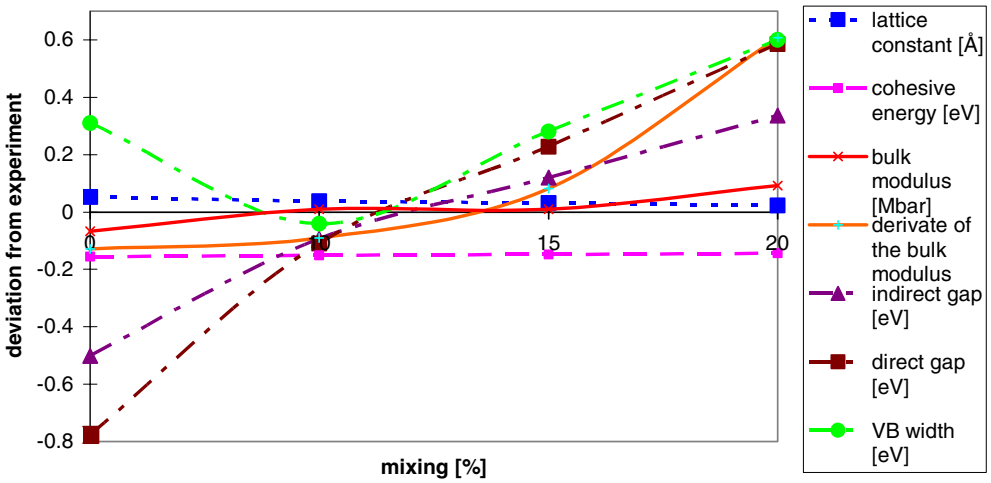

Figure 1. Dependence of the deviation of the calculated lattice constant, cohesive energy, bulk modulus and its pressure derivative, as well as of the indirect and direct gap, and the valence band width of silicon from the experimental values, as a function of the percentage of exact exchange mixed with the GGA exchange.

Table 2. The properties of bulk silicon calculated with 12% mixing of exact exchange into GGA, as compared with the experimental data, and with 'traditional' plane-wave LDA calculations.

	Lattice constant (Å)	Cohesive energy (eV)	Bulk modulus (Mbar)	VB width (eV)	Indirect gap (eV)	Direct gap (eV)
12% mixing	5.466	−4.95	0.99	12.65	1.16	4.21
Exptl. [21]	5.431	−4.75	0.99	12.5	1.17	4.19
Plane wave LDA	5.433	−4.84 [22]	0.92	12.2	0.5 [23]	2.5

of silicon are still well reproduced. For this purpose, we have investigated the dependence of the properties of bulk silicon on the mixing percentage of HF exchange into the so-called PBE potential of GGA [18], using the CRYSTAL'2003 code with norm-conserving Barthelat–Durand pseudopotentials [19] and a Gaussian basis (double-ζ plus polarization functions: 21G*), optimized to these pseudopotentials for the valence electrons [20]. Figure 1 shows the results.

The rough power-function fitting to the data points show that the well known overbinding (too negative cohesive energy) and overestimation of the lattice constant of DFT is not very sensitive to the mixing. On the other hand, both the elastic constants and the parameters characterizing the quality of the electronic structure have optimum values in the 10–15% range. The best agreement with experiment can be obtained at 12%.

Table 2 shows the calculated values compared to experimental data [21] and to traditional LDA calculations [22, 23]. As can be seen, the structural and elastic data fit the experimental values about the same way as the traditional plane wave LDA results (which are better converged in terms of the basis set). At the same time the electronic structure obtained with the hybrid functional gives excellent agreement with experiment. It should be emphasized that not only is the indirect (minimum) gap reproduced well, but also the relative energies in the conduction band are correct and, at the same time, the valence band-width has also improved.

These results show that our one-parameter hybrid functional gives an adequate description of the perfect crystal. In order to check whether defect properties are also well reproduced, we have selected the donor state of the hydrogen interstitial. Since the bond centre configuration of hydrogen does not change between the neutral and the positive charge state (and the relaxation is also relatively small), the one-electron energy level occupied in the neutral charge state should be close to the position of the (+/0) occupation level (i.e. the Fermi level position, where the charge state changes). The latter has been measured experimentally by deep level transient spectroscopy (DLTS) to be at $E_V + 0.96$ eV [24]. The calculation with 12% mixing results in 0.90 eV. This shows that the method is capable of correctly predicting defect levels as well. (Pure GGA gives $E_V + 0.46$ eV.)

The CRYSTAL code has the additional advantage of also treating core electrons of an atom explicitly, and it also allows for mixing all-electron and pseudopotential + valence electron treatments for different atoms. This feature makes the *first principles* calculation of the hyperfine (hf) interactions of the defect spin with neighbouring atoms (as measured by magnetic resonance spectroscopy) possible, without using a frozen core approximation. This will be utilized in the hf calculations.

In the following we will show that, in critical cases, where LDA or GGA fail, the hybrid functional approach results in an equilibrium configuration of the correct symmetry. Still, usage of the exact exchange means the calculation of all exchange integrals: a process scaling with the fourth power of the number of electrons. This makes geometry optimization very costly. Therefore, in our large-scale electronic structure calculations for BICs, we have pre-relaxed the defect structures using pure GGA. For that purpose the very fast SIESTA code has been used [25].

SIESTA implements DFT combined with the pseudopotential approximation, and uses numerical atomic orbitals (NAOs) as a basis set. It is aimed at large-scale calculations with linear-scaling simulations but is also capable of employing conventional diagonalization methods. In this work, only the latter capability was used. Norm-conserving pseudopotentials have been generated according to the Troullier–Martins [26] scheme, in the Kleinman–Bylander [27] separable form. Core radii of 1.78 and 1.89 bohr were used for B and Si, respectively. The program requires the use of a grid to compute some of the contributions to the matrix elements and total energy and also for performing the Fourier transforms needed to evaluate the Hartree potential and energy by solving Poisson's equation in reciprocal space. A grid—fine enough to represent plane waves with kinetic energy up to 90 Ryd—has been used. Calculations have been carried out using the same GGA functional [18] as with CRYSTAL. The NAO basis set also consisted of double-ζ plus polarization functions. The maximum extent of these functions was 5.965 Å. Structural relaxations have been performed by means of the conjugated gradient algorithm until the forces were smaller than 0.04 eV Å^{-1}. In order to keep the usage of resources within the available framework without compromising the predictive power of the results, careful convergence tests had been carried out [4]. Based on those results, all calculations were done in a 64-atom supercell, using a 2^3 Monkhorst–Pack (MP) k-point set [28] in the Brillouin zone (BZ) summation.

Table 3 shows the calculated formation energy of the BICs at their equilibrium geometry, compared to the values of Windl *et al* [2]. The good agreement shows that the same configuration was found for each BIC. Consequently, hybrid functional calculations were carried out with the CRYSTAL code in the same supercell, using the same MP set.

Although the formation energies are near convergent, the interaction of the repeated defects still causes a significant dispersion in the defect levels. The positions of the levels of an isolated defect can be estimated using a tight binding retrofit [29].

Table 3. Comparison of BIC formation energies obtained with the 2^3 MP set in the present SIESTA calculations (using localized numerical atomic orbitals, as basis, and norm-conserving pseudopotentials) with those obtained with the 4^3 MP set of the VASP calculation of Windl *et al* [2] (using plane waves, as basis, and ultrasoft pseudopotentials), both within the GGA approximation. The values contain no corrections (those of Windl *et al* have been obtained from their figure 1 by subtracting the charge correction). The formation energies have been calculated with respect to Si_i and B_s^-.

BIC	Present	Windl *et al* [2]
	64-atom cell 2^3 MP set	64-atom cell, 4^3 MP set
B^-	0.00	0.0
BI^+	−0.69	−0.5
BI_2	−2.30	−2.3
BI_3^+	−4.36	−4.8
B_2^{2-}	+0.76	+0.6
B_2I	−1.71	−1.7
B_2I_2	−2.74	−2.7
B_2I_3	−5.54	−5.7
B_3I^-	−2.67	−2.7
B_3I_2	−3.69	−3.6
$B_3I_3^-$	−6.30	−6.3
B_4I^{2-}	−1.92	−2.1
B_4I_2	−5.00	−4.9
$B_4I_3^-$	−6.68	−6.5

3. Results on the B_s + V and B_s + Si_i defects

Two basic boron-related defect centres, G10 [5] and G28 [6], have been extensively investigated in the past experimentally. Although the results are far from conclusive, it is interesting to see what the hybrid functional calculations result in for these defects.

The G10 EPR centre, having a curiously low C_1 symmetry, was assigned to a second nearest neighbour pair of a boron substitutional (B_s) and a vacancy (V). Watkins has argued that the nominal C_{1h} symmetry of such an arrangement is distorted into C_1 because of a pseudo Jahn–Teller effect (see figure 2(a)). The t_2 level of an undistorted vacancy splits upon the C_{1h} perturbation by the second neighbour B atom in such a way that the two lower lying levels are in close proximity. This causes the further distortion from C_{1h} to C_1. The symmetry and the assignment has later been confirmed by ENDOR; however, it is rather mysterious why a first neighbour pair is not the preferred configuration for this defect.

Our calculations predict the first neighbour pair to be lower in energy by 0.18 eV. (It should be noted though, that the 64-atom supercell, used in the present study, is certainly too small for giving a convergent energy difference for two configurations with rather different spatial extension.) The equilibrium symmetry of both configurations is C_{1h}! For the second neighbour pair the first two defect levels with β spin (unoccupied) above the VB edge are within 0.05 eV of each other. This finding supports the assumption of Watkins about a likely pseudo Jahn–Teller effect. That cannot be taken into account in a 0 K calculation, which is then bound to end up with C_{1h} symmetry. For the first neighbour pair the same difference is only 0.005 eV (the next state being 0.3 eV higher). This indicates that the nominally C_{3v} symmetry of this configuration (see figure 2(b)) causes a splitting of the t_2 state of the vacancy into a lower lying e and a higher lying a_1 state. The occupation of the e state by one electron causes

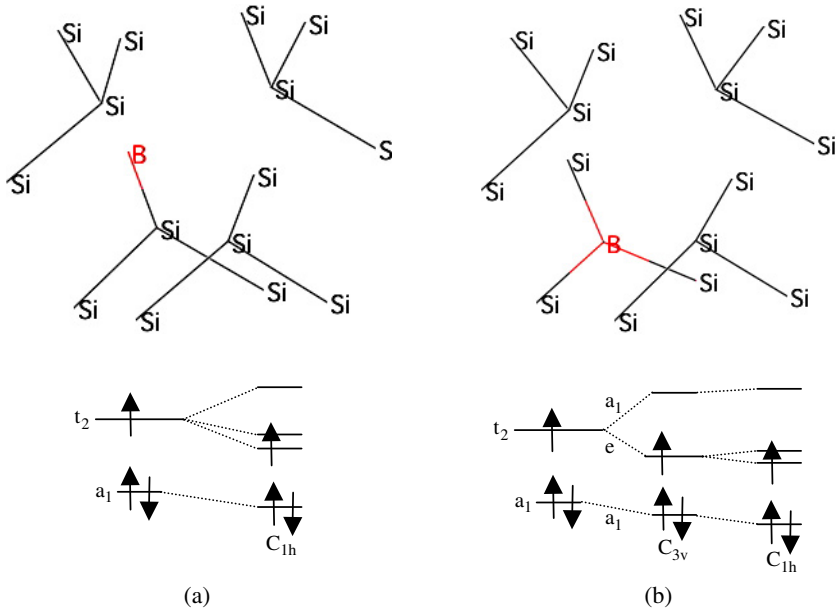

Figure 2. Symmetry and level splitting in the second neighbour (a) and first neighbour (b) B–V pair.

Table 4. Measured and calculated hyperfine parameters for the BV defect (in MHz). The four highest silicon hyperfine interactions are shown.

	G10 [5] Measured by ENDOR (MHz)			Second neighbour B–V Calculated (MHz)			First neighbour B–V Calculated (MHz)		
	A_1	A_2	A_3	A_1	A_2	A_3	A_1	A_2	A_3
B(11)	0.541	0.537	0.459	2.0	1.5	1.2	7.4	5.4	4.9
Si-1	393.9	249.9	247.8	320.0	193.5	193.1	355.4	206.1	205.6
Si-2	67.2	56.8	55.2	59.7	50.0	48.6	79.1	66.5	65.3
Si-3	63.1	53.4	51.9	60.1	49.4	48.2	77.6	65.1	63.9
Si-4	36.1	23.6	23.1	20.6	9.7	9.7	23.6	17.2	16.9

a static Jahn–Teller distortion into C_{1h} (from which the symmetry could be lowered further by a pseudo Jahn–Teller effect.) That makes the first neighbour pair also a good candidate for G10!

The calculated hyperfine parameters for the first and second neighbour pair are very similar (see table 4). As expected there is some difference in the amount of localization on the boron atom, with a lower value in the case of the second neighbour pair. However, the accuracy of the hyperfine calculation does not allow a clear-cut judgment, whether the first or the second neighbour pair should be assigned to the G10 centre. Both have similar characteristics, and both sets of results are in reasonable agreement with the measured data. We are inclined, however, to assign the observed signal to the energetically more favourable, and by any means more 'natural' first neighbour B–V pair, resolving a long-standing mystery. We emphasize that this is only possible on the basis of an accurate calculation of the electronic structure, showing that the first neighbour pair has C_{1h} symmetry at $T = 0$ K, instead of C_{3v}, with a likely distortion to C_1 for finite temperatures. The singly occupied level of the first neighbour B_s + V pair is at $E_V + 0.25$ eV. Convergence tests on larger cells are in progress.

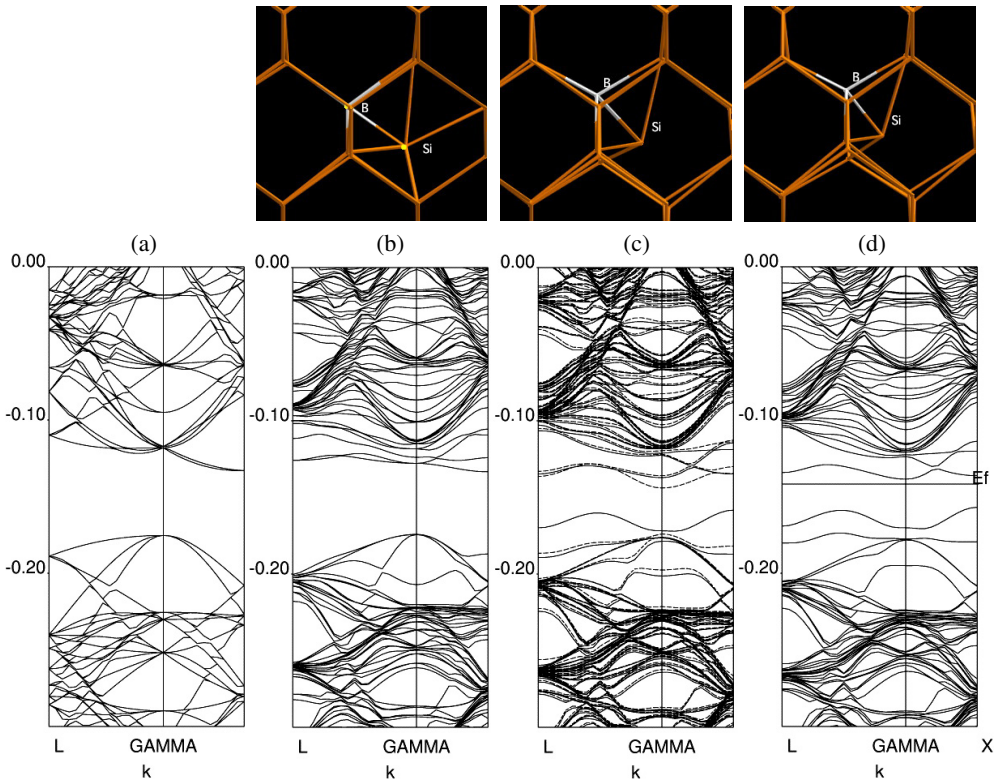

Figure 3. The electronic structure of BI $= B_s + Si_i$ in the C_{3v} positive (b) in the C_{1h} neutral (c) and in the C_{1h} negative (d) charge state, compared with the band structure of the perfect Si_{64} supercell (a). In case of open shell systems solid (dashed) lines show states with $\alpha(\beta)$ spin. Energy values are in Hartree (0.1 H $=$ 0.3675 eV). (Note that the primitive BZ is back-folded to the BZ of the supercell: twice in the L [111] and four times in the [100] direction.) The line marked E_F separates occupied and unoccupied states.

The G28 EPR centre and the corresponding DLTS peaks were assigned to a BI pair [6]. Recently, the so-called *R* infrared (IR) centre was also tentatively assigned to a BI $= B_s + Si_i$ defect [4, 30]. However, the BI defect is a bistable complex with negative *U* behaviour[4]: the occupation levels are at $E(+/0) = E_V + 0.99$ eV and $E(0/-) = E_V + 0.75$ eV. The reverse order means that the neutral charge state is never stable in equilibrium, and the defect changes from the positive charge state directly to the negative one at $E_F = E_V + 0.88$ eV. Therefore, the G28 centre can only be detected in non-equilibrium EPR experiments (e.g. under illumination), for EPR measures the paramagnetic neutral charge state. The observed hf interactions imply a defect with C_{1h} symmetry.

Previous theoretical studies have found [30–33], indeed, that the BI defect is bistable. In the (+) charge state it consists of a Si_i at the tetrahedral site, next neighbour to a B_{Si}. This defect has C_{3v} symmetry (see figure 3(b)). In the (−) charge state, a [110] split interstitial configuration with C_{1h} symmetry is preferred (see figure 3(d)). In the (0) charge state both

[4] The name, negative-*U*, refers to the apparent negative Coulomb energy for two holes ((+) charge state) or two electrons ((−) charge state) which seems to make them energetically favoured over the neutral charge state. In fact, the negative-*U* behaviour is due to the energy gained by strong relaxation of the nuclei, leading to different configurations of the defect in the different charge states.

Table 5. Comparison of the occupation levels calculated by different methods for the BI defect with the DLTS results for the G28 centre. Values are given (in eV) with respect to the valence band edge.

	LDA [32]	LDA [30]	GGA [33]	Present GGA	Experiment [6]
Correction	None	Empirical	Scissor (+ charge correction)	Based on level positions in hybrid functional calc.	
(+/0)	0.66	1.07	1.1	0.94	0.99
(0/−)	0.55	0.79	0.7	0.66	0.75
(+/−)	0.61	0.93	0.9	0.80	0.87

Table 6. Measured and calculated hyperfine parameters for the BI defect in (10^{-4} cm^{-1}).

	G28 [6]			BI		
	A_1	A_2	A_3	A_1	A_2	A_3
B(11)	21.5	4.2	4.1	34.2	17.8	17.6
Si-1	37.5	24.3	24.3	32.5	14.7	14.5
Si-2	19.0	0.0	0.0	22.6	10.5	10.5

configurations constitute local minima of the total energy surface. So far, all calculations have predicted the C_{3v} configuration to be more stable (by 0.21 eV in LDA and by 0.07 eV in GGA) than the C_{1h} one in the neutral state—in contrast to the experimental observation. This has always been suspected [32] to be the consequence of the band gap error.

We have optimized the geometry of the BI defect in both the (+), and the (−) charge state using our hybrid functional with the CRYSTAL code. The obtained geometries did not deviate significantly from those obtained in a pure GGA calculation with SIESTA. However, in the neutral charge state the C_{1h} configuration (figure 3(c)) was found to be more stable by 0.14 eV than the C_{3v}—in agreement with experiment.

The electronic structure resulting from the hybrid functional calculations are also shown in figure 3. For comparison the band structure of the perfect crystal is given in the BZ of the supercell. In all cases the top of the VB is not very much disturbed, showing that the supercell is big enough to accommodate the defect. Still, for the C_{1h} configurations, the dispersion of the highest occupied defect state is considerable. The level position of the isolated defects can be estimated by the tight binding retrofit to $E_V + 0.42$ eV and $E_V + 0.46$ eV for the neutral and the negative charge state, respectively.

One-electron levels can be directly linked to defect-to-band photoluminescence, but none has yet been assigned to the BI defect. Only occupation levels are known (from DLTS), which require the comparison of the energies of the neutral and the charged states, which is not yet possible in the present CRYSTAL version. Therefore, we have used the positions of occupied states obtained here with respect to the VB edge, and corrected the GGA total energies, obtained with SIESTA, accordingly. The results are shown in table 5. It can be stated that our procedure is at least as effective as other correction schemes in predicting DLTS results. It should be emphasized, however, that the agreement confirms that the hybrid functional calculation results in good one-electron level positions, while giving the correct total energy sequence among various configurations in the neutral state. Hopefully, the CRYSTAL code will soon become capable of directly calculating the occupation levels as well. It should be noted here that, unlike in [33], we have not applied any correction for the charged supercells, since a present study of ours [34] indicated that the usually applied procedure introduces a larger error than what it corrects.

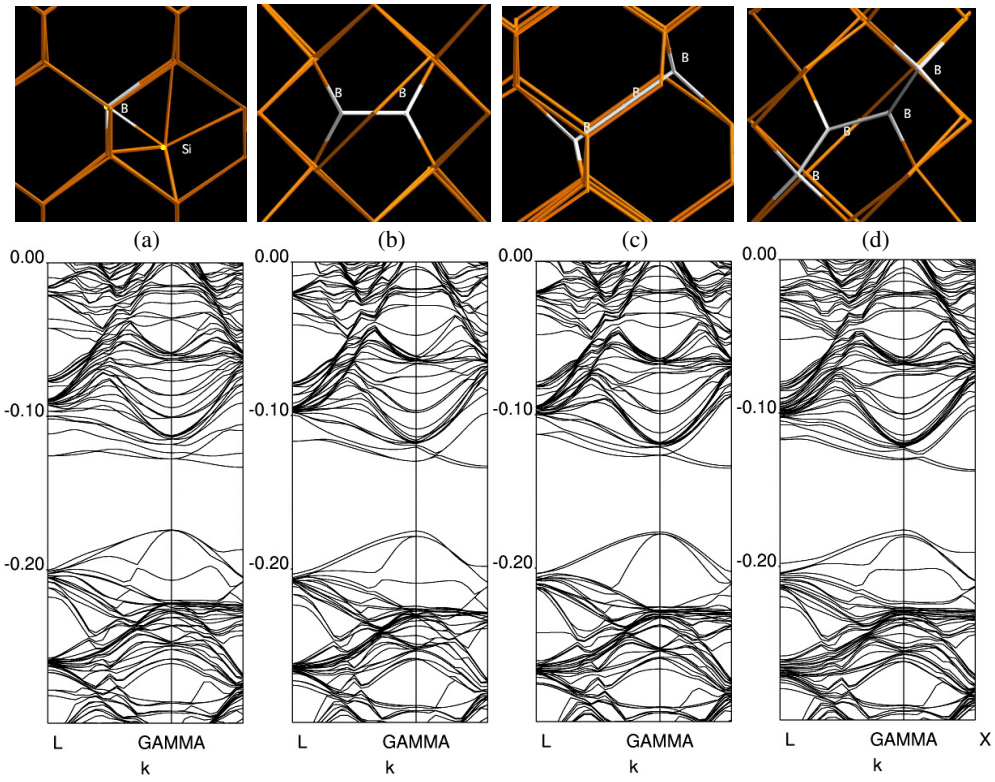

Figure 4. The electronic structure of (a) $BI^{+} = (B_s + Si_i)^{+}$, (b) $B_2I^0 = (B_2)^0_s$, (c) $B_3I^{-} = (B_s + B_i + B_s)^{-}$, and (d) $B_4I^{2-} = (B_s + (B_2)_s + B_s)^{2-}$ in the BZ of the supercell.

Having obtained the symmetry of the neutral charge state with the hybrid functional calculation in agreement with G28 centre, the hf data can also be compared. This is shown in table 6. Again, the localization on the boron atom is somewhat overestimated, but—within the accuracy of the hf calculation—the character of the centre is well reproduced.

4. Electronic structure of the BICs

For comparison of their formation energy, BICs had been considered earlier [1, 2] in their stable charge state relevant to the case when the Fermi level is pinned at midgap (corresponding to the situation after implantation), as shown in table 3. We have calculated the electronic structure for these states, except for B_3I_2, where the hybrid functional calculation clearly indicates that the singly negative charge state should be stable if the Fermi level is pinned to midgap (the position of the highest, doubly occupied level is at $E_V + 0.40$ eV).

The electronic structure of the BICs fall into two categories. In the first one, the boron atoms (which are always negatively charged but may be compensated by interstitial Si) introduce delocalized, occupied effective mass states very near the VB edge (the distance falling within the error bar of the calculation). The BIC series B_n^{n-} and BI^{+}, B_2I^0, B_3I^{-}, B_4I^{2-} fall into this category. Loss of activation occurs only due to the compensating effect of the self-interstitial in the latter series. It should be noted that the clusters $(B_s)_2^{2-}$, and $(B_s)_3^{3-}$ have positive formation energies with respect to the isolated B_s^{-} (see table 3 and [2]), obviously because of the repulsion of two negatively charged B atoms. With the hybrid functional

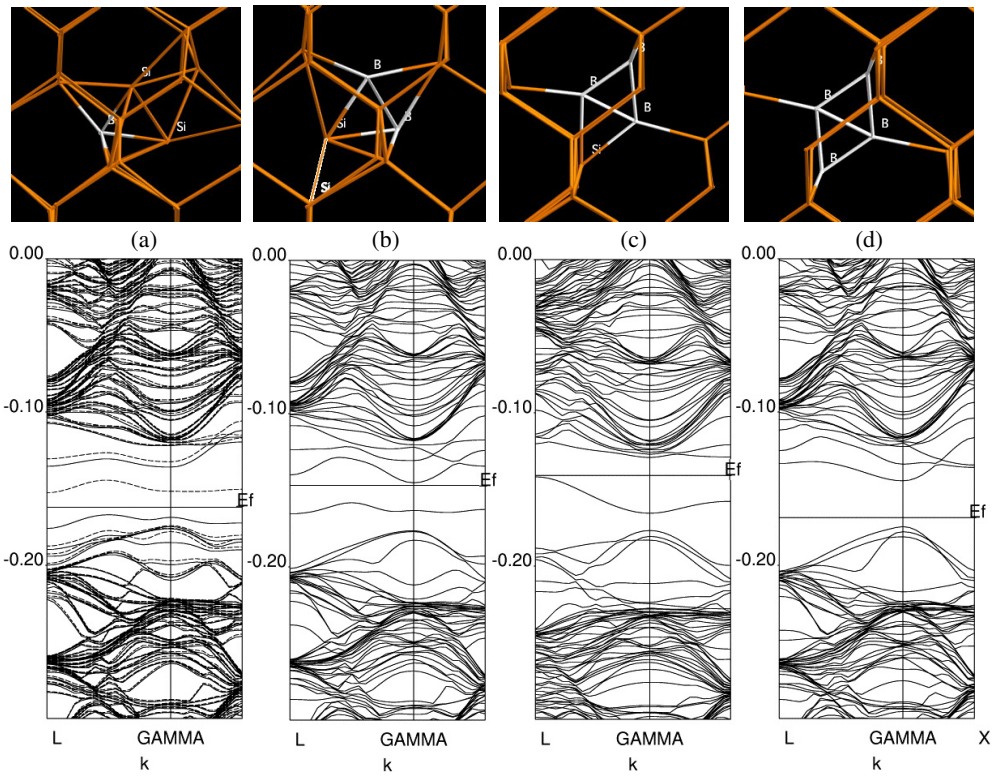

Figure 5. The electronic structure of (a) $BI_2^0 = (B_s + 2Si_i)^0$, (b) $B_2I_2^0 = [(B_2)_s + Si_i]^0$, (c) $B_3I_2^- = (B_s + 2B_i)^-$, and (d) $B_4I_2^0 = (B_s + 2B_i + B_s)^0$ in the BZ of the supercell. The line marked E_F separates occupied and unoccupied states. Solid lines: spin-up, dashed lines: spin-down states.

we find, however, that a $(B_s)_2^0$ complex, in which the boron atoms relax back into the plane of their respective three Si neighbours into an sp^2 configuration and are not bonded to each other, is energetically favoured over isolated B_s^0 atoms. This fact may be used to explain why $(B_s)_2^{2-}$ complexes can after all be observed by infrared spectroscopy (see [4] and references therein). It is known that boron diffuses as a neutral interstitial, and becomes substitutional by the kick out reaction $B_i^0 => B_s^- + Si_i^0 + h^+$, or $B_s^- + I^+$. A divacancy having captured a boron atom forms the $BV = (B_s + V)^0$ defect. A B_i^0 atom may find this complex (no Coulomb repulsion), forming a stable $(B_s + B_s)^0$ complex which will consequently trap two electrons but can no longer dissociate because of the high barrier for dissociation. The electronic structures of the B_nI series are shown in figure 4. The EMT states are within 0.1 eV of the VB edge.

The second category of BICs introduces localized states in the band gap. The electronic structures are shown in figures 5, 6. The estimated positions of the isolated defect levels are given in table 7. As can be seen, these states are not too deep for the B_nI_3 series (figure 6) and are likely to be filled even after annealing. In contrast, the B_nI_2 series introduces states near midgap (figure 5), and are likely to become empty when annealing of the intrinsic defects causes the lowering of the Fermi level. Therefore, this is the class of BICs which impair the activation rate the most.

The results given in table 7 indicate that, based on the electronic structure, it will be difficult to distinguish between BICs containing the same number of interstitials and different number

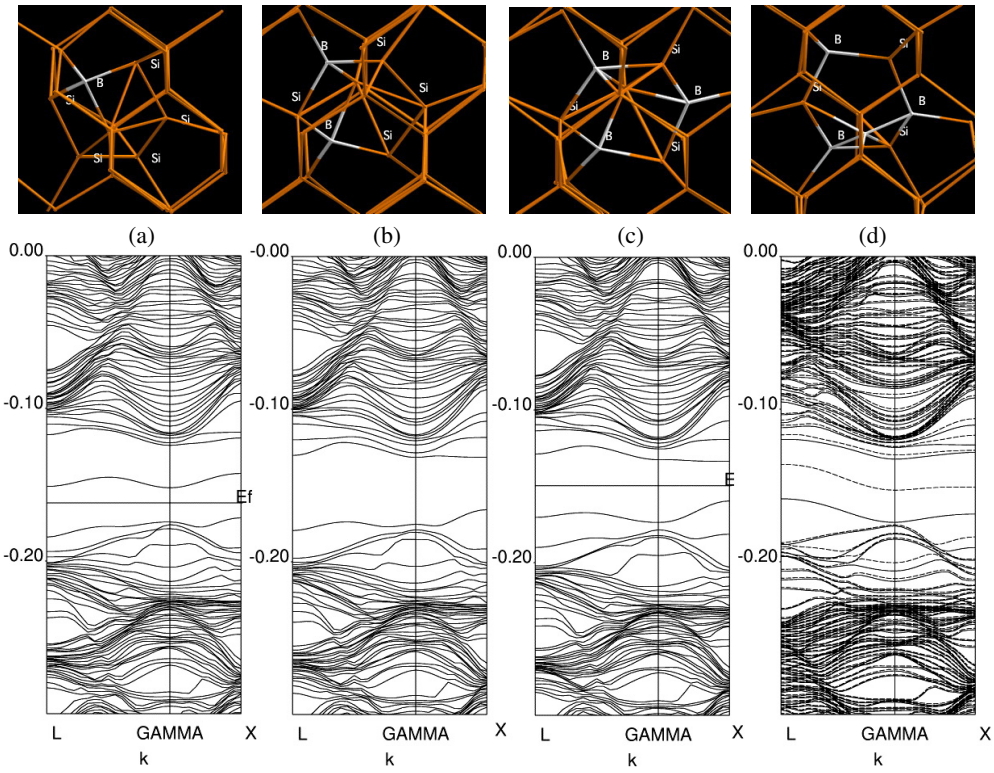

Figure 6. The electronic structure of (a) $BI_3^+ = (B_i + 2Si_i)^+$, (b) $B_2I_3^0 = [2B_i + Si_i]^0$, (c) $B_3I_3^- = (B_i + 2Si_i)^-$, and (d) $B_4I_3^- = (B_s + 3B_i)^-$ in the BZ of the supercell. The line marked E_F separates occupied and unoccupied states. Solid lines: spin-up, dashed lines: spin-down states.

Table 7. Estimated level position of isolated B_nI_m clusters with respect to the VB edge (in eV). Always the highest occupied localized acceptor state is given for the charge state relevant to a Fermi level pinned to midgap.

	$n = 1$	$n = 2$	$n = 3$	$n = 4$
$m = 1$	<0.1	<0.1	<0.1	<0.1
$m = 2$	0.53	0.47	0.40	∼0
$m = 3$	∼0	0.07	0.22	0.14

of boron atoms. On the other hand, if recent suggestions about the average value of $m/n \approx 1$ get confirmed, the diagonal of table 7 shows clear differences among the possible compositions.

5. Summary

We have shown that a one-parameter hybrid functional is capable of the accurate calculation of the whole electronic structure *and* the elastic properties of crystalline silicon, and at the same time can provide dependable defect level positions in the gap. Using this method we have investigated the boron + vacancy and boron + self-interstitial centres in detail, giving a consistent description of the experimentally observed G10 and G28 centres. We also report the electronic structure of all the boron-interstitial clusters (BICs) which may affect the activation

rate of boron implantation. We find that B_nI_2 clusters, with deep acceptor states just below midgap, can be the main source of decrease in the activation rate. In contrast, B_nI clusters cause shallow EMT states. B_nI_3 clusters lie between these two sets.

Acknowledgments

This work has been carried out in the framework of the EU FP5 IST-2000-30129 project 'FRENDTECH-EAST', using the resources of the supercomputer centre HLR Stuttgart. The authors are grateful for fruitful discussions with N T Son. The help of P Pichler and G Battistig is also appreciated.

References

[1] Caturla M J, Johnson M D and Diaz de la Rubia T 1998 *Appl. Phys. Lett.* **72** 273
Lenosky T J, Sadigh B S, Theiss K, Caturla M J and Diaz de la Rubia T 2000 *Appl. Phys. Lett.* **77** 1834
Zhu J, Diaz de la Rubia T, Yang L H, Malhoit C and Gilmer G H 1996 *Phys. Rev.* B **64** 4741
Zhu J 1998 *Comput. Mater. Sci.* **12** 309
[2] Windl W, Liu X-Y and Masquelier M P 2001 *Phys. Status Solidi* b **226** 37
Liu X-Y, Windl W and Masquelier M P 2000 *Appl. Phys. Lett.* **77** 2018
[3] Alippi P, Ruggerone P and Colombo L 2004 *Phys. Rev.* B **69** 125205
[4] Deák P, Gali A, Sólyom A, Ordejón P, Kamarás K and Battistig G 2003 *J. Phys.: Condens. Matter* **15** 4767
[5] Watkins G D 1976 *Phys. Rev.* B **13** 2511
Sprenger M, van Kemp R, Sieverts E G and Ammerlaan C A J 1987 *Phys. Rev.* B **35** 1582
[6] Watkins G D 1975 *Phys. Rev.* B **12** 5824
Harris R D, Newton J L and Watkins G D 1987 *Phys. Rev.* B **36** 1094
[7] Rubio A, Corkill J L, Cohen M L, Shirley E L and Louie S G 1993 *Phys. Rev.* B **48** 11810
[8] Städele M, Moukara M, Majewski J A, Vogl P and Görling A 1999 *Phys. Rev.* B **59** 10031
[9] Furthmüller J, Cappellini G V, Weissker H-Ch and Bechstedt F 2002 *Phys. Rev.* B **66** 045110
[10] Baraff G A and Schlüter M 1984 *Phys. Rev.* B **30** 1853
[11] Gerstmann U, Gali A, Deák P, Overhof H and Frauenheim Th 2004 *Mater. Sci. Forum* **457–460** 711
[12] Becke A D 1993 *J. Chem. Phys.* **98** 5648
Becke A D 1997 *J. Chem. Phys.* **107** 8554
[13] Lee C, Yang W and Parr R G 1988 *Phys. Rev.* B **37** 785
[14] Muscat J, Wander A and Harrison N M 2001 *Chem. Phys. Lett.* **342** 397
[15] Dovesi R, Orlando R, Roetti C, Pisani C and Saunders V R 2000 *Phys. Status Solidi* b **217** 63
[16] Saunders V R, Dovesi R, Roetti C, Orlando R, Zicovich-Wilson C M, Harrison N M, Doll K, Civalleri B, Bush I, D'Arco Ph and Llunell M 2003 *CRYSTAL2003 User's Manual* University of Torino
[17] Gali A, Deák P, Ordejón P, Son N T, Janzén E and Choyke J W 2003 *Phys. Rev.* B **68** 125201
[18] Perdew J P, Burke K and Ernzerhof M 1997 *Phys. Rev.* B **77** 3865
Perdew J P, Burke K and Ernzerhof M 1997 *Phys. Rev.* **78** 1396
[19] Barthelat J C and Durand P 1977 *Mol. Phys.* **33** 159
[20] Causá M, Dovesi R and Roetti C 1991 *Phys. Rev.* B **43** 11937
[21] Madelung O (ed) 1991 Data in science and technology *Semiconductors* (Berlin: Springer)
[22] Chang K J and Cohen M L 1987 *Phys. Rev.* B **35** 8196
[23] Zunger A and Cohen M L 1979 *Phys. Rev.* B **20** 4082
[24] Holm B, Bonde Nielsen K and Bech Nielsen B 1991 *Phys. Rev. Lett.* **66** 2360
[25] Artacho E, Sánchez-Portal D, Ordejón P, García A and Soler J M 1999 *Phys. Status Solidi* b **215** 809
[26] Troullier N and Martins J L 1991 *Phys. Rev.* B **43** 1993
[27] Kleinman L and Bylander D M 1982 *Phys. Rev. Lett.* **48** 1425
[28] Monkhorst H J and Pack J K 1976 *Phys. Rev.* B **13** 5188
[29] Aradi B 2003 *Thesis* Budapest University of Technology and Economics
[30] Adey J, Goss J P, Jones R and Briddon P R 2003 *Phys. Rev.* B **67** 245325
[31] Windl W, Bunea M M, Stumpf R, Dunham S T and Masquelier M P 1999 *Phys. Rev. Lett.* **83** 4345
[32] Hakala M, Puska M J and Nieminen R M 2000 *Phys. Rev.* B **61** 8155
[33] Jeong J W and Oshiyama A 2001 *Phys. Rev.* B **23** 5204
[34] Gerstmann U, Deák P, Rurali R, Aradi B, Frauenheim Th and Overhof H 2003 *Physica* B **340–342** 190